Helicopter Aerodynamic Loading in the Airwake of a Moving Ship

Nicholas Fernandez
Ph.D. Student

Ieuan Owen
Professor

Mark D. White
Professor

University of Liverpool
Liverpool, UK

Alanna Wall
Senior Research Officer

Richard Lee
Research Officer

Weixing Yuan
Senior Research Officer

National Research Council Canada
Ottawa, Canada

ABSTRACT

This paper presents an analysis of the unsteady aerodynamic loading of a helicopter immersed in the airwake of a generic destroyer undergoing several ship motion types: static, sinusoidal pitching, regular 2-DOF, and realistic irregular 3-DOF ship motions. The study was a collaborative effort between the National Research Council Canada and the University of Liverpool, where each organization have applied their respective modelling approach (whether by simulation or experiment). It was shown that whilst there were only marginal differences in the mean helicopter loads for each motion type, the effects of ship motion are more apparent in the RMS loads, and the instantaneous load and air-velocity spectra. Dominant peaks in the thrust load spectra, as well as subsequent second and third harmonics, are shown at the ship motion frequency for sinusoidal pitching and regular 2-DOF ship motions, which have been attributed to the interaction between the turning rotor and the moving ship. This analysis provides a foundation for understanding the relationships between ship airwake and helicopter loading, and for extending that understanding to impacts on flight operations.

1 Introduction

The helicopter-ship dynamic interface (HSDI) presents one of the more challenging flying environments that a pilot can encounter (Ref. 1), where they have to contend with the unsteady turbulent air flow in the wake of the ship superstructure, i.e., the ‘airwake’, as well as a moving deck and possibly degraded visual cues. There has been a considerable international research effort towards gaining a greater understanding of the HSDI using modelling and simulation (M&S) to aid in the development of helicopter-ship operational guidelines, ship design and pilot training (Ref. 2). One of the challenges in M&S of the HSDI is ship motion. Until recently, research into the effects of ship motion upon the airwake has been limited, partly by computational capabilities. However, the combination of methods for modelling ship dynamics and for including moving boundaries within computational fluid dynamics (CFD) means that M&S can now be used to investigate the impact of ship motion upon the air flow over the ship. With this in mind, the NATO Research Technology Group AVT-315 (Ref. 3) was established to assess the M&S methods used for shipboard helicopter operations, with a particular emphasis on the influence ship motion has upon ship airwake, and the resultant impact on the helicopter and pilot. The influence of ship motion on airwakes for different computational approaches, including a literature review of other related work, can be found in Ref. 3.

This paper discusses elements of the research undertaken within AVT-315, more specifically those which investigate the aerodynamic loading of a helicopter immersed in a ship airwake. The purpose of the paper is to demonstrate how helicopter aerodynamic loading is affected by the ship airwake in the presence of ship motion, whether by a simulated approach or by wind-tunnel experiment. Research undertaken by both the University of Liverpool (UoL) and the National Research Council (NRC) Canada is presented. UoL's contributions focus upon the application of the Virtual AirDyn (VAD), a software-based airwake-dynamometer, whereby helicopter six-component loading is quantified with an aircraft flight dynamics model immersed in a CFD-generated airwake (Ref. 4). The NRC has undertaken an experimental wind tunnel testing campaign where their Helicopter Unsteady Loads Measurement System (HULMS) was employed to measure unsteady rotor thrust loading, a metric which has shown good correlation with pilot workload (Refs. 5, 6). By comparing helicopter loading in the airwake of a model ship with and without motion, the impact of motion upon the helicopter (and by extension the pilot) was assessed and an evaluation of the significance of ship motion on helicopter operations made.

2 Helicopter-Ship platform

This research has made use of the NATO Generic Destroyer (NATO-GD), shown in Figure 1, and the NATO Generic Rotorcraft (NATO-GR). These models were developed as part of AVT-315 to enable the HSDI research community to undertake collaborative research using the common platforms. The NATO-GD is representative of a modern destroyer with a characteristic continuous slab-sided superstructure with typical features such as a bulky mast, exhaust stack and radar. The NATO-GR is based on a Sikorsky SH-60B Seahawk, a medium-lift multi-role maritime helicopter used by the US Navy, amongst others. The diameter of the main rotor was specified for AVT-315 as 53 ft 8 in (16.36 m), and the mass of the aircraft is specified at 15,432 lb (7,000 kg).

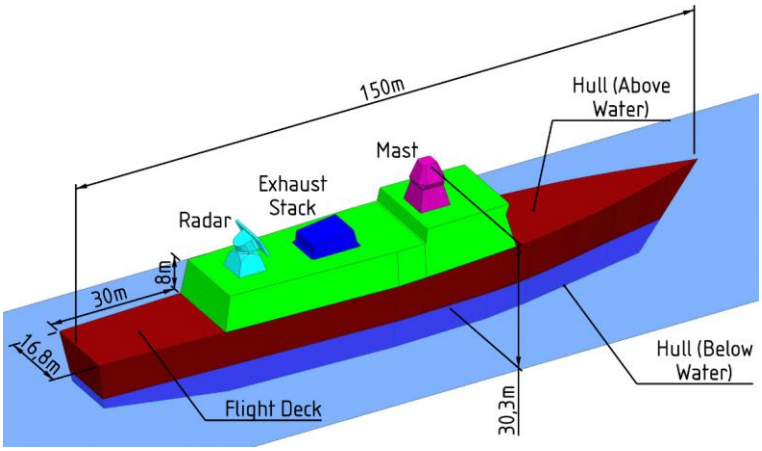

Figure 1: NATO-GD ship model.

These vehicle models were presented in Ref. 3 alongside a set of computed realistic ship motion profiles for the NATO-GD. Three ship motion cases were examined in this study and compared against a static ship: a sinusoidally pitching ship, a regular two-degrees-of-freedom (2-DOF) ship motion and a realistic irregular 3-DOF ship motion. The sinusoidal pitching motion is described in Equation 1, where for the full-scale (FS) motion profile the ship motion amplitude, θ_a = 5 ° and frequency, f = 0.04 Hz. The regular ship motion case, shown in Figure 2, was calculated for an ideal seaway with single-frequency unidirectional waves coming from ahead that resulted in sinusoidal motions in pitch and heave, which are out of phase with one another. The motion is approximately representative of a seaway with a significant wave height of 2 m and a dominant wave period of 15 s. The realistic ship motion profile, shown in Figure 3, was computed for the ship moving at 15 kt (7.72 m/s) through a sea-state 5

(SS5) (defined in Ref. 7) with waves approaching from ahead. The seaway was simulated as having a significant wave height of 4 m and a dominant wave period of 12 s. For each motion type, the ship displacements are described about the center of gravity (c.g.) of the ship, which has also been specified in Ref. 3.

$$\theta = \theta_a \sin(2\pi f) \quad \textbf{(1)}$$

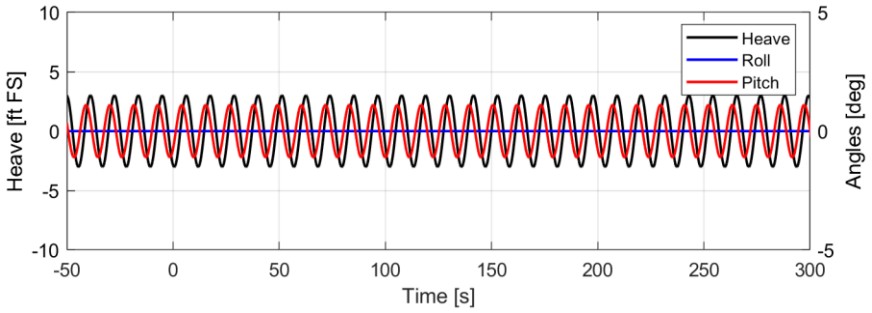

Figure 2: Regular 2-DOF ship motion profile in FS.

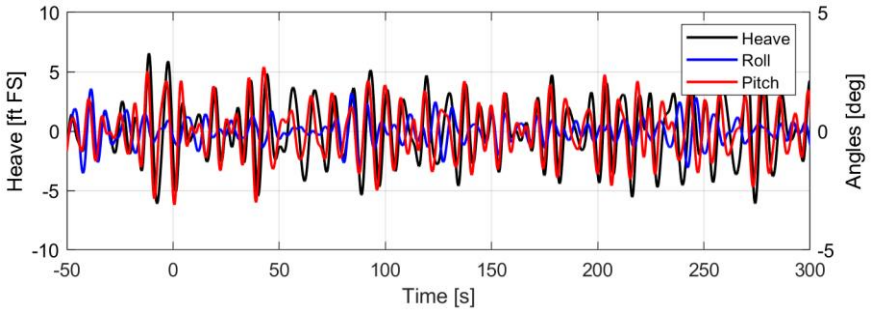

Figure 3: Realistic ship motion profile for wave conditions of SS5 from ahead in FS.

The measurements that are presented in this work were made at several locations over the deck of the NATO-GD. The HULMS experimental approach was mainly applied at a nominal 'high hover' (HH) position, which placed the helicopter's c.g. at hangar height and the center of the rotor hub directly over the landing spot (at the center of the deck). The HH position approximately places a pilot's eyeline at hangar height, where a pilot would safely hold hover until a decision is made to land the helicopter; and corresponds to a rotor height of 7.5 in (0.19 m) above the deck at model-scale (MS) (9.5 m FS). Longitudinally, the HH position places the center of the rotor hub 11.8 in (0.3 m) MS (15 m FS) aft of the hangar face, on the deck centerline.

The unsteady helicopter loads from the VAD analysis were computed for the aircraft fixed at a series of locations over the deck of the ship, ranging from one deck-width off the port side of the deck to over the starboard side of the ship, passing through the landing spot. The locations of the test points are illustrated in Figure 4, where each point indicates the location of the helicopter c.g. The height of the helicopter c.g. was again placed at hangar height, as was used in the NRC HULMS experiments. This set of test point locations was selected as it is representative of the lateral traverse maneuver of the UK Royal Navy port-side approach for helicopter recovery.

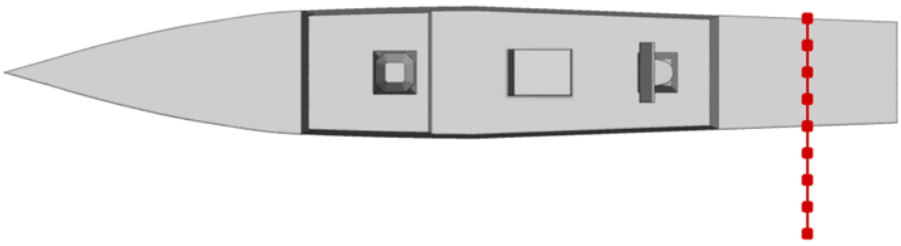

Figure 4: VAD test point locations over the NATO-GD flight deck.

3 Flight Modelling Approach

The analysis of helicopter aerodynamic loads undertaken by UoL was carried out using the VAD (Ref. 4). This approach integrates CFD generated ship airwakes, computed by NRC for this study, with a flight dynamics model to quantify the unsteady air loading on a helicopter fixed in position and immersed in the ship airwake.

3.1 CFD Ship Airwake Generation

The open-source CFD code, OpenFOAM, was used to compute the three-dimensional unsteady incompressible flow over the NATO-GD ship. The OpenFOAM pressure-based Navier-Stokes solver, *pimpleFoam*, was used in this study. Because of the nature of bluff-body aerodynamics, Delayed Detached Eddy Simulation (DDES) was employed to model turbulence. The computations were performed for the model at FS (150 m long ship). Unstructured grids were used near the ship (above water), except in the airwake where a structured grid block was employed, generating a hybrid mesh. The grid spacing in the ship airwake was 10 in (25 cm). As a result, the final grid contained approximately five million cells. The freestream velocity was set to 40 kt (≈ 20 m/s) in the computations. The freestream turbulence intensity was set to 0.65%, consistent with the wind tunnel experiments for the motion cases. The second-order linear-upwind scheme was used for the motion cases. A timestep of 0.001 s was adopted, which resulted in a maximum Courant-Friedrichs-Lewy (CFL) number of ~0.1 in the ship airwake over the flight deck. Further details of the methods can be found in Ref. 8.

OpenFOAM has several motion functions to define the boundary or body motions. The ‘tabulated6DOFMotion’ function was used with pre-generated tabulated motion schedules. The solid-body motion solver was used in this study without deforming boundaries as other solvers were developed for some other specific conditions and applications. The flow and motion solvers were validated against wind tunnel and sea trial data for the Canadian Patrol Frigate (Ref. 9). All three motion types and the static ship are considered in this paper.

3.2 The Virtual AirDyn

The software used to implement the flight dynamics model was Advanced Rotorcraft Technology Inc.’s FLIGHTLAB software (Ref. 10), which allows the creation of a flight dynamics model using a library of pre-defined components. The aircraft flight model used for the trial was the FLIGHTLAB generic rotorcraft, reconfigured to be representative of the NATO-GR. The helicopter components include a blade-element model for the four-bladed main rotor, a Bailey disc tail-rotor model, a finite-state Peters-He dynamic inflow model, a turbo-shaft engine model, load coefficient lookup tables for each of the aerodynamic surfaces and fuselage, a flight control system with a stability augmentation system, and a landing gear model.

The velocity components within the ship airwake and the motion of the ship were integrated with the flight dynamics model using Simulink. The airwakes were first extracted from the CFD calculations onto a Cartesian grid and

converted into a MATLAB data lookup table, with variables x, y, z, u, v, w and time. The flight dynamics model requires the airwake velocity components to be applied to 46 Airload Computation Points (ACPs) distributed around the aircraft. The locations of the ACPs are shown in Figure 5 as red dots: ten along each main rotor blade with the remainder at the aircraft's c.g., the vertical tail, the tail rotor hub and the starboard and port stabilizers. As the aircraft is moved around in space, the Simulink model receives the location of each of the ACPs from the flight dynamics model and uses the lookup tables to interpolate the velocity components at each of the ACPs and then returns the airwake variables back to the flight dynamics model.

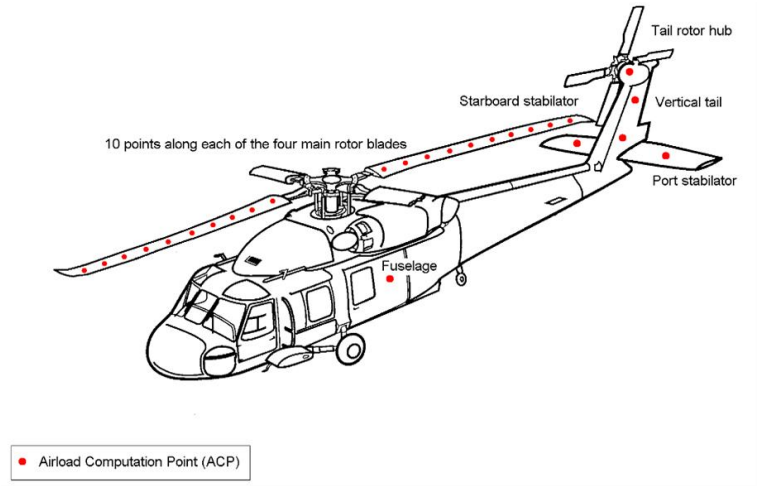

Figure 5: Airload Computation Points in the flight dynamics model (extracted from Ref. 4).

Prior to measurements being recorded, the aircraft model was trimmed in the undisturbed freestream wind (away from the influence of the ship airwake). When the flight dynamics model is held fixed, and immersed in the ship airwake, the loads are inherently unbalanced. It is these unbalanced loads that are computed by the VAD. The unsteady air loads are applied across the helicopter ACPs, illustrated in Figure 5; these are then summed at the aircraft c.g. in each of the six axes.

4 Experimental Methodology

The modelling and simulation approach used at NRC is known as the Shipboard Helicopter Operational Limit (SHOL) Analysis and Simulation (SHOLAS) Analysis Methodology (SAM) (Ref. 5). The SAM toolkit is the product of a collaboration between the NRC, Defence Research and Development Canada, and the Department of National Defence. Wind tunnel testing is one of the primary airwake analysis tools used at the NRC.

4.1 Wind Tunnel Testing Facility

For this study, the NRC 3 m x 6 m Wind Tunnel was used. The test section of this open-circuit wind tunnel, with the lower-floor insert installed, is 10.2 ft (3.1 m) wide, 17.7 ft (5.4 m) high and 21.0 ft (6.4 m) long. The insert ramp is characterized by a no-slip roughness that results in a significant boundary layer near the floor. The NATO-GD tests, by agreement with the AVT-315 working group, were conducted in the absence of turbulence spires. Figure 6 shows the background mean flow speed and turbulence level for the flow in the 3 m x 6 m Wind Tunnel with the insert ramp and no spires. The flow speed values are normalized by the reference tunnel wind speed collected at the reference height, which is equivalent to 64.0 ft (19.5 m FS; 0.39 m MS). For the data collected under this study, the wind tunnel reference speed was set to a nominal value of 19 kt (10 m/s).

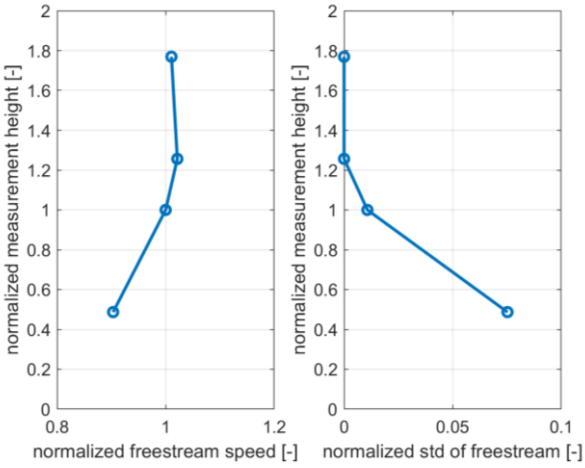

Figure 6: Background mean flow speed and turbulence level in the wind tunnel.

To accommodate studies involving ship motion, the wind tunnel was modified to include a motion system. The ship-motion system consists of a 6-DOF motion platform under the wind tunnel floor, a model spine, a fabric support ring, and a fabric cover. A product of Symetrie, the NOTUS hexapod is a Stewart platform which provides motion in six degrees-of-freedom.

4.2 Measurement and Instrumentation

NRC uses a combination of flow measurements and unsteady loading measurements. Flow measurements are often used together with HULMS data to provide information about ship airwakes. For flow measurements, the Series 100 Cobra-probes used by NRC are fast-response, four-hole pressure probes that provide dynamic, three-component velocity and static pressure measurements up to a maximum speed of 107 kt (55 m/s) within an acceptance cone of 45 degrees. The probe features a multi-faceted head containing four pressure taps, each connected to a pressure transducer located nearby in the body in the probe. The close proximity of the pressure transducers, in combination with the short tubing, allows data to be recorded at 1.5 kHz. The test setups with the Cobra-probes are shown in Figure 7 and more details on these measurements are available in Ref. 11.

(a) **(b)**

Figure 7: Test setup for ship motion experiments in the NRC 3 m x 6 m Wind Tunnel. The two Cobra-probe configurations are shown (a: moving, b: stationary) on the NATO-GD model, 1:50 scale.

Unsteady load measurements are accomplished using the HULMS. The conventional HULMS setup focuses on the interaction between the wind and superstructure, and the resulting effects on aerodynamic loads on the helicopter. An instrumented rotor (and sometimes a fuselage) model (1:50 scale) is placed in a hover position behind an equivalent scale model of the ship mounted in the wind tunnel, where the rotor is turning to create a representative downwash. The model rotor and fuselage capture both the mean and root mean square (RMS) aerodynamic loading. For the work associated with AVT-315 the rotor-only HULMS setup, shown in Figure 8, was used because the NRC have previously demonstrated approximate correlations between the unsteady rotor thrust and pilot ratings (Ref. 5).

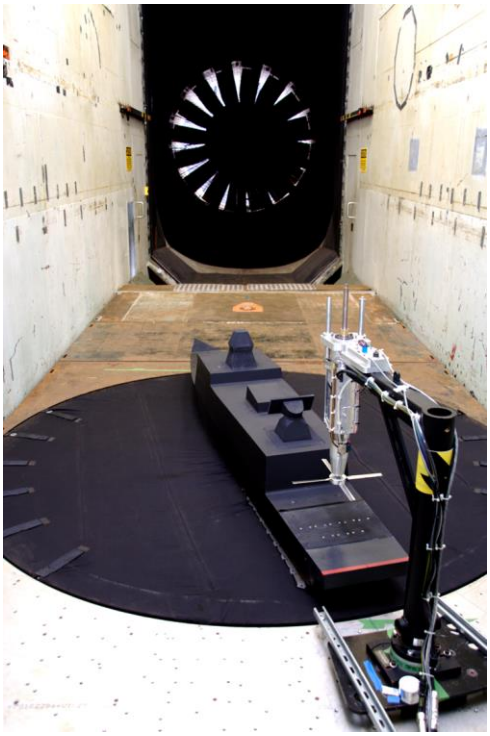

Figure 8: Test setup for ship motion experiments in the NRC 3 m x 6 m Wind Tunnel. The rotor-only HULMS is shown behind the NATO-GD model, 1:50 scale.

The HULMS rotor-only instrumentation suite comprised a dynamic balance which measured the aerodynamic loading acting on the scaled rotor model, an encoder to monitor rotor speed, two orthogonally-aligned accelerometers to monitor the vibration of the rotor support system, and thermocouples to sense the surface temperature of the drive motor and the rotor balance.

The unsteady aerodynamic loading acting on the rotor model was sensed by a Model 20E12A load sensor, developed by JR3 Inc. (Figure 9). The rotor balance is a fast-response six-component load sensor which senses three orthogonal components of force (drag, side force, and thrust) and moment (pitching, yawing, and rolling). Its compact puck-shaped size enabled the balance to be placed close to the rotor plane so that the fluctuating load sensed by the balance was dominated by the unsteady aerodynamic load of the rotor, rather than being affected by other influences such as the aerodynamic loading arising from the motor casing. A distinguishing feature of the Model 20E12A is an annular opening that passes from the ground-side to the live-side of the balance. The annulus allows a rotor shaft spinning at high rotational speed to pass through the balance and deliver mechanical power to the rotor, as the balance senses the fluctuating aerodynamic load developed by the rotor.

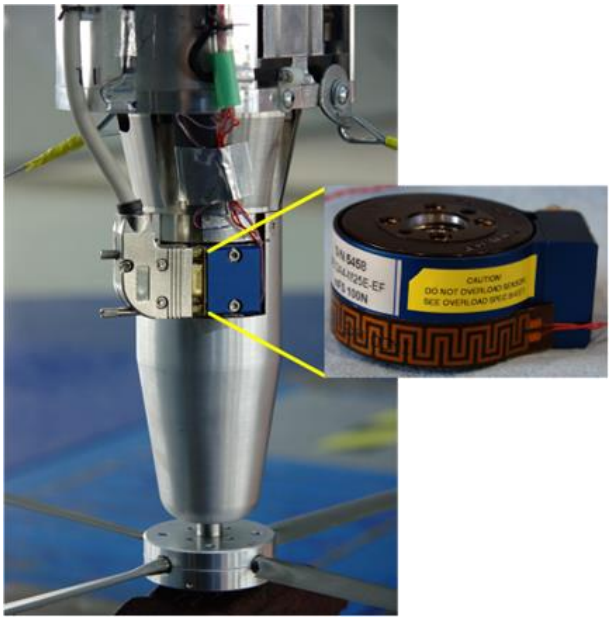

Figure 9: The rotor balance (JR3 Model 20E12A).

The rotor used for this study was a 1:50 scale model that approximates the downwash of a CH148 Cyclone rotor (four blades) with a diameter of 14 in (0.35 m). This rotor was selected because the NRC already had the model from previous projects and its size was close to that of the NATO-GR which is 13 in (0.32 m) at MS. The Cyclone is the maritime helicopter operated by the Royal Canadian Air Force.

4.3 Scaling and Experimental Design

Experimental scaling for HULMS tests is based on matching the appropriate rotor downwash to incoming flow speeds, in addition to respecting reduced frequency scaling (Ref. 6). Using actuator disc theory (Ref. 12), the velocity scale (λ_V) can be shown to be related to model rotor thrust as follows:

$$\lambda_V = \frac{V_m}{V_p} = \sqrt{\frac{T}{W_0}\frac{1}{\lambda_\rho}} \cdot \frac{1}{\lambda_D} \tag{2}$$

where V_m represents the velocity at model scale, and V_p is the velocity at prototype scale; and where T represents measured MS rotor thrust, W_o is the weight of a prototype FS helicopter, λ_ρ is the density scale (assumed to be unity throughout this investigation), and λ_D is the geometric scale. The frequency scale (λ_f) can be obtained by reduced frequency with geometric and velocity scales:

$$\lambda_f = \frac{\lambda_V}{\lambda_D} \tag{3}$$

Furthermore, it can be shown that the force (λ_F) and moment (λ_M) scales are expressed, respectively, as:

$$\lambda_F = \frac{F_m}{F_p} = (\lambda_D \cdot \lambda_V)^2 \quad \textbf{(4)}$$

$$\lambda_M = \frac{M_m}{M_p} = \lambda_D \cdot \lambda_F \quad \textbf{(5)}$$

where F_m and F_p are forces at model and prototype scale, respectively; and similarly with the moments, M_m and M_p. For force spectral densities (S_F) and moment spectral densities (S_M), the scale factors are:

$$\lambda_{S_F} = \frac{\lambda_f}{\lambda_F^2} \quad \textbf{(6)}$$

$$\lambda_{S_M} = \frac{\lambda_f}{\lambda_M^2} \quad \textbf{(7)}$$

Thus, the mean measurement of the thrust developed by the model rotor is critical for establishing the velocity, frequency, force and moment, and spectral-density scales for the experiment.

4.4 Test Procedures

Wind tunnel data for both the HULMS and Cobra-probes were collected for three of the four motion types presented in this paper: static ship, sinusoidal motion, and regular ship motion. The case with realistic motion for SS5 could not be collected due to kinematic limitations of the motion platform. The time series of rotor thrust, which is the component that has been demonstrated to date to be of greatest importance for assessing workload, are processed according to the scaling described earlier. For this experiment, the center of the rotor hub was placed at the nominal HH location as described earlier. The support structure for the HULMS was fixed to the wind tunnel floor behind the turntable. For a limited number of runs at headwinds, a single Cobra-probe was mounted behind the flight deck as shown in Figure 10. This single probe was installed to understand any difference in airwake frequency content as a result of the turning rotor. The nominal rotor speed was 8,000 rpm (which was selected to avoid contamination of the loading data with structural resonant frequencies in the mounting system), and 120 s of loading data were collected at 625 Hz.

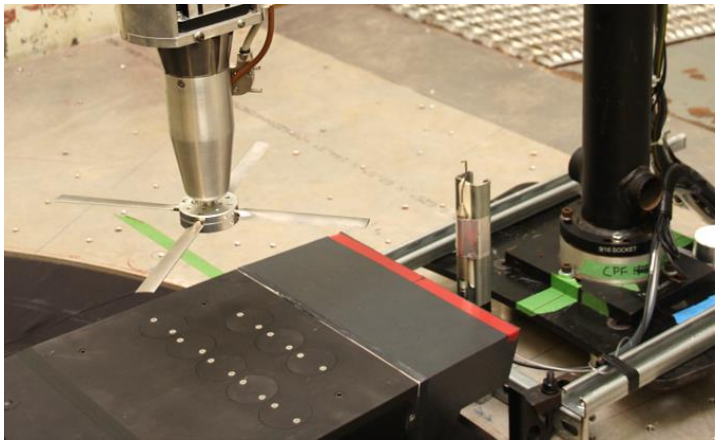

Figure 10: Cobra-probe fixed behind the NATO-GD flight deck with the rotor-only HULMS installed.

5 METRICS – UNSTEADY LOADS

Unsteady loads as a conceptual metric for pilot workload have been used by both the NRC and UoL. Fuselage and rotor models, physical and computational, have been used to integrate the fluctuating loading over their surfaces and can be considered as an 'airwake probe' used to assess the magnitude of the disturbances caused by the ship airwake that the pilot must overcome.

The metrics that are output from the HULMS and VAD analyses are the mean and RMS of the unsteady helicopter loads (forces and moments). The mean of the loads in each axis is computed directly from the unsteady time series. However, the RMS of the unsteady loads is not calculated using the conventional definition; instead, it is defined as the square root of the integral of the power-spectral-density (PSD) of the unsteady loads between the FS frequency limits of 0.2 to 2 Hz, as illustrated in Figure 11. This analysis technique accounts for the fact that although the unsteady loads are imposed over a very wide frequency range, the high-frequency loads (> 2 Hz) are less important because the inertia of the aircraft means it does not respond significantly, while the lower frequency loads (< 0.2 Hz) can be counteracted by the pilot through the helicopter's controls. Loads in the frequency range 0.2 to 2 Hz are said to be in the closed-loop pilot response frequency range (Ref. 13) and have the greatest influence on pilot workload. In general terms, the RMS loading is responsible for the pilot workload while the mean loads will influence the control margins.

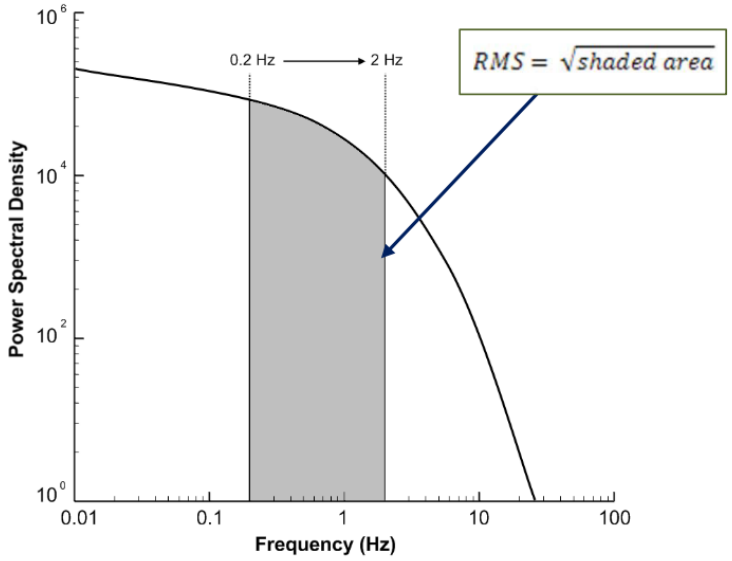

Figure 11: Method of computing the RMS loads using the closed-loop pilot response frequency range (extracted from Ref. 4).

The 0.2 to 2 Hz frequency range has been used traditionally for studies that did not include ship motion; however, in the case of extra energy due to ship motion at frequencies below 0.2 Hz, it is still unclear whether pilot workload would be impacted (Ref. 14). For integrated values in this paper, the frequency range of 0.2 to 2 Hz will be maintained and investigation of the ship motion-related energy below the 0.2 Hz limit will be done in a separate study to hypothesize whether it should be considered to change the integration limits in the future.

For the measurements collected with the HULMS, before spectral windowing can be used to calculate the RMS loads, a fitted spline in the frequency range of interest must be calculated. This step is necessary because the loads

are affected by small resonant peaks that are known to be structural resonances in the HULMS equipment; the spline is fitted to filter these peaks from the spectral data. An example of a spline fit to the spectrum is shown when discussing the spectrum analysis in a later section. Following these processing steps, the spectra and RMS rotor thrust at FS are then available for analysis.

6 Results and Discussion

The results of the analysis, from both the VAD and HULMS measurements, are presented in the following sections where the unsteady loads have been assessed in terms of the mean and RMS (0.2 to 2 Hz) statistics, and the spectra of instantaneous loads and air-velocity.

6.1 Mean and RMS Helicopter Loads

The results from the VAD analysis are shown in Figure 12 and 13, where the mean and RMS loads in each of the six load axes are plotted against the normalized lateral location of the flight dynamics model relative to the deck landing spot, y/B (where positive y/B is toward the starboard side). The normalization distance, B, is the width of the flight deck at its longitudinal mid-point and the dimensional coordinate, y, follows the ship's lateral axis with an origin located on the ship's deck landing spot. This comparison was made to assess the effects of motion type upon helicopter loading, i.e., a static ship, a sinusoidal pitch, a regular motion with heave and pitch components (no roll), and a realistic irregular 3-DOF motion.

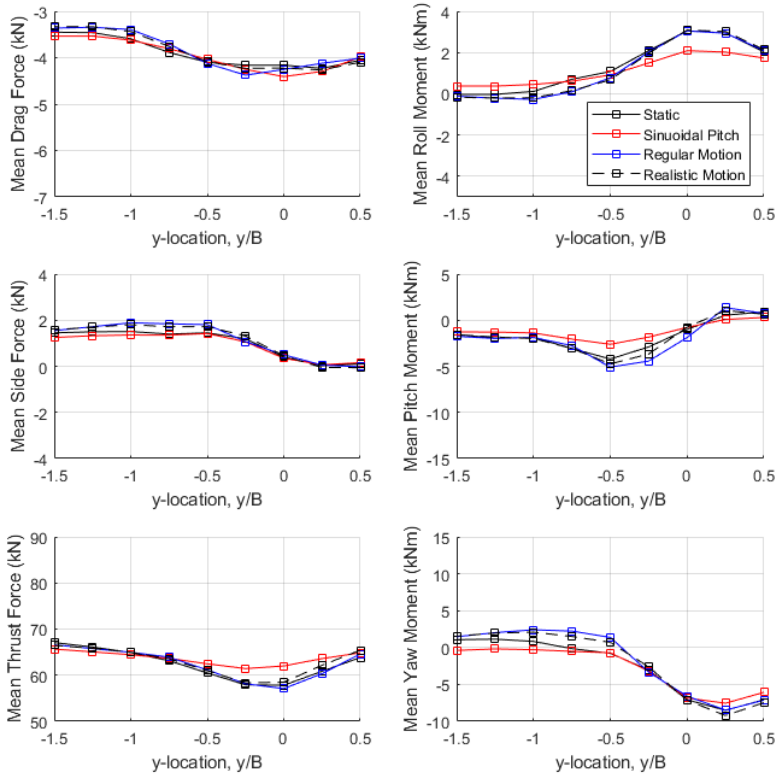

Figure 12: Comparison of mean helicopter air loads from the VAD analysis for a ship undergoing various motion types: static, sinusoidal pitch, regular 2-DOF and realistic irregular 3-DOF ship motions.

First, considering the general wind loading characteristics, the loads presented in Figures 12 and 13 are given in the body reference frame of the helicopter, which means that if the helicopter has a non-zero attitude, then the load

reference frame is also rotated with the airframe. When the aircraft is trimmed in the freestream headwind, the main rotor is tilted slightly to counteract the sideways thrust of the tail rotor and the freestream drag. This means that the drag and side forces do not approach zero in the locations where the wind conditions would be freestream, instead the loads approach the trim load value. It is also shown that the loads are not symmetrical about $y/B = 0$ despite a reasonably symmetrical airwake; this is due to the direction of rotation of the main rotor blades causing asymmetrical loading (the retreating blade will experience a much lower relative incident velocity from the airwake than will the advancing blade).

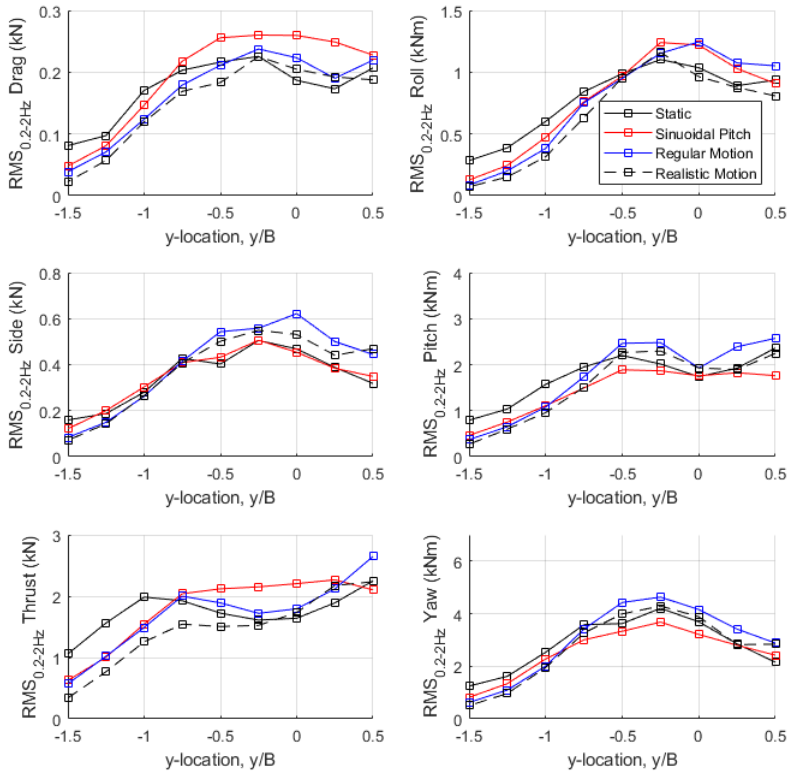

Figure 13: Comparison of RMS helicopter air loads from the VAD analysis for a ship undergoing various motion types: static, sinusoidal pitch, regular 2-DOF and realistic irregular 3-DOF ship motions.

It is shown, in Figure 12, that for all motion cases the aircraft experiences deficits in thrust and drag whilst directly over the deck and immersed in the ship airwake. The drag reduction occurs because of the reduced wind speed in the lee of the superstructure, previously shown in Ref. 15, and the recirculation zone would act to 'pull' the aircraft forwards towards the ship hangar. The thrust deficit over the deck suggests that a greater collective control input would be required and is due to the downdraft over the deck in a headwind. Similarly, there are also variations in the side force, and in the roll, pitch and yaw moments as the aircraft translates across the deck; all loads which would need to be counteracted in the aircraft controls to maintain position over the deck. In Figure 13, it is generally shown that the RMS loads across all axes are greatest when the aircraft model is immersed in the ship airwake: the peak RMS loads occur whilst the aircraft model is positioned directly over the deck (-0.5 < y/B < 0.5). In the regions where the air flow is close to freestream, i.e., y/B = -1.5, the RMS loads tend toward zero as the air flow in these regions is less disturbed.

When comparing between the various motion types, it is seen in Figure 12 that there are only marginal variations in the mean loads between each motion type. There is a slightly greater deviation for the sinusoidal pitch cases (particularly in the thrust, roll and pitch axes) when compared with all other motion types; however, the deviations from the general trend are not large and there is not one motion type that shows a consistently higher/lower trend across all axes. In contrast, Figure 13 shows that motion type does have a clear impact upon the RMS loads as differences of 10-20% are observed between the cases. However, there is again no consistent trend across all load axes where one particular motion type shows greater RMS loads.

Next, considering the main rotor loading only (i.e., not including the fuselage, empennage, and aerodynamic surfaces from the VAD analysis), the mean and RMS rotor loads are shown in Table 1 for each ship motion type for both the HULMS and VAD measurements. The position of the rotor for these measurements is the HH position. The differences between the two analysis approaches become apparent: in the HULMS method, the normalization of the loads results in equal mean thrust values for each motion type; whereas for the VAD, the mean thrust shows variation between motion type as this approach quantifies the thrust deficit relative to freestream conditions. The HULMS without the fuselage is known to record slightly higher levels of unsteady rotor thrust than with the presence of the fuselage. A correction on the order of -0.002 to the HULMS normalized RMS thrust (not applied in Table 1) is appropriate for comparing the values.

It is shown, in Table 1, that there are some variations in the RMS thrust loads between motion types, which is consistent with those shown in Figure 13. The RMS loads have also been normalized by mean rotor thrust loads for the purpose of comparing between the two analysis approaches. It is shown that whilst there is a difference between the HULMS and the VAD approach, the overall magnitude of the normalized RMS loads between motion types is similar; on the order of 0.03. The sinusoidal pitch ship motion shows the greatest normalized RMS thrust loads, which may be attributed to this motion type having the largest deck displacements, whilst the static ship shows the smallest, as was shown in Figure 13 at the $y/B = 0$ position. The regular and irregular ship motion types, which both have more than one DOF, show a lesser RMS loading than the sinusoidal pitch, and the irregular motion type shows the lesser of the two. Therefore, although there is some variation in the RMS thrust between the methods for each case, they show similar trends and similar orders of magnitude.

Table 1: Mean and RMS rotor trust measured by the HULMS and VAD at the HH position.

	HULMS Thrust			VAD Thrust		
Motion Type	Mean (N)	RMS (N)	RMS /Mean	Mean (N)	RMS (N)	RMS /Mean
Static	68670	2392	0.0348	57380	1651	0.0288
Sinusoidal Pitch	68670	2542	0.0370	61341	2181	0.0356
Regular Motion	68670	2496	0.0363	56707	1812	0.0320
Realistic Motion	-	-	-	58057	1760	0.0303

6.2 HULMS Spectral Analysis

The PSD of the unsteady rotor thrust (F_Z) at the nominal HH location is shown in Figure 14 for the headwind case with no ship motion. The fitted spectrum used to determine the windowed RMS thrust, and to remove the known structural frequency response from the windowed RMS thrust, has also been shown. The spectra of the total velocity (U) measured by the Cobra-probes at four locations are shown: HH and points 6 m equivalent FS on the port and starboard sides for the Cobra-probes fixed in space; and HH for the Cobra-probes fixed to the moving deck (Figure 10). The figure reveals a similar shape for all data sets, with broadband turbulence throughout and no motion or vortex-shedding peaks.

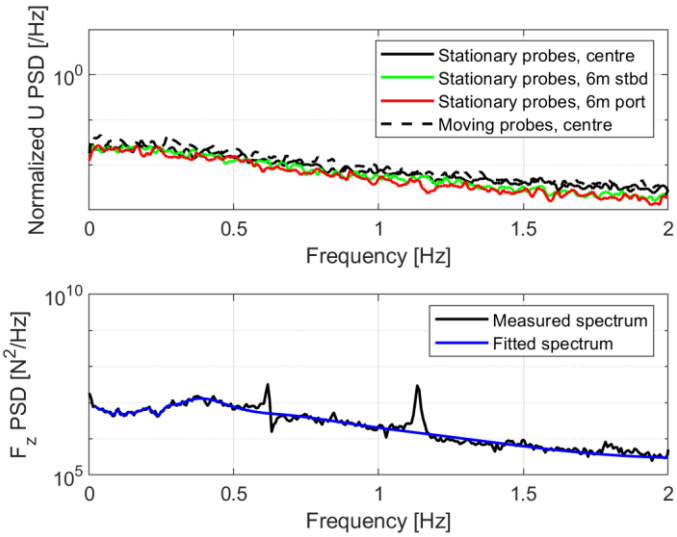

Figure 14: Comparison of Cobra-probe (top) and HULMS (bottom) spectra at the nominal HH location in headwind for a static ship. Values are presented at equivalent FS.

Figure 15 shows the data for the headwind case with sinusoidal pitch. In the top image, a strong peak associated with the ship motion at 0.04 Hz (dominant wave period of 25 s) can be seen in all the Cobra-probe data, a feature which is mirrored in the HULMS data. Based on this data, it appears that the HULMS works effectively as an 'airwake probe' to capture the main features in the airwake. The extra area under the first motion peak in the HULMS data is on the order of 2,500 N, which is similar to the area under the fitted curve between 0.2 to 2 Hz. For cases with significant loading due to ship motion, it should be investigated whether some of this energy impacts pilot workload.

Similarly, Figure 16 shows a dominant peak in both the flow velocity and the thrust loads at the 2-DOF ship motion frequency (significant wave period of 15 s), albeit at a smaller magnitude, owing to the lower magnitude of the ship motion. In this case, the area under the first motion peak is on the order of 1,500 N, which is less than the area under the fitted curve between 0.2 to 2 Hz. Therefore, this demonstrates that whilst the differences in mean and RMS loads are reasonably small, for simple ship motions such as this the effects of motion are more clearly shown in the frequency content of the airwake. Whilst the HULMS approach could not be applied to the realistic irregular ship motion case in this analysis, due to kinematic limitations of the motion base, it has previously been shown in Ref. 3 that when energy is added to the airwake over a more broadband range of frequencies, no peak is shown in the spectra of the velocity over deck. Based upon the evidence presented so far, it may therefore be assumed that no significant peak would be present in the rotor thrust spectra for irregular ship motions. If no significant motion

peaks are present for unsteady loading for realistic ship motion cases, then it follows that the integration range of 0.2 to 2 Hz is appropriate.

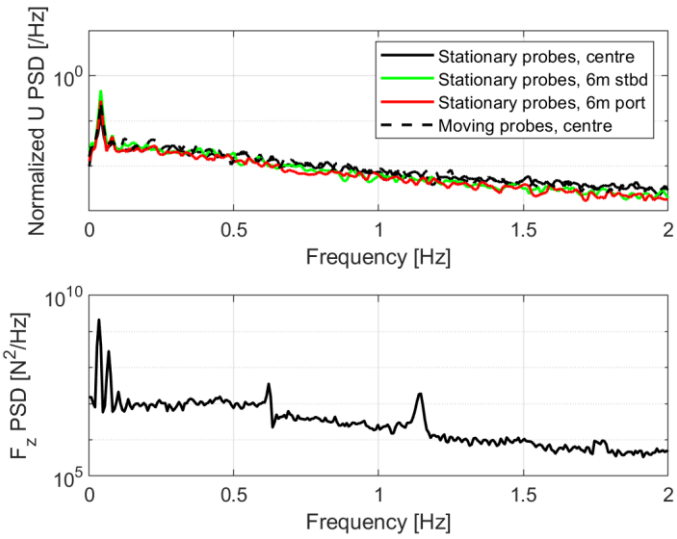

Figure 15: Comparison of Cobra-probe (top) and HULMS (bottom) spectra at the nominal HH location in headwinds for a sinusoidally pitching ship. Values are presented at equivalent FS.

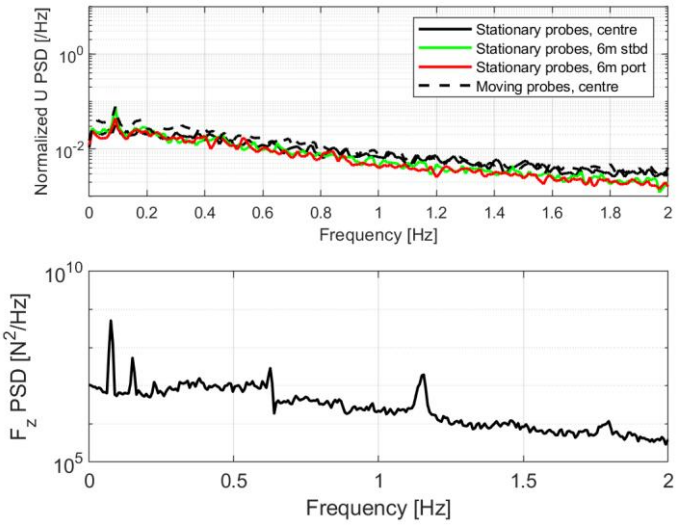

Figure 16: Comparison of Cobra-probe (top) and HULMS (bottom) spectra at the nominal HH location in headwinds for the regular ship motion case. Values are presented at equivalent FS.

Interestingly, Figures 15 and 16 show a feature in the HULMS data that is not present in the Cobra-probe data: the existence of frequency peaks of superharmonics at twice and three times the motion frequency. Since the set-ups used to collect the Cobra-probe data and the HULMS data were fundamentally different, and the rotor was not present for the Cobra-probe measurements, it was hypothesized that the harmonics resulted from an interaction between the turning rotor and the moving deck. To investigate this, a Cobra-probe was placed behind the flight deck in the rotor wake (Figure 10). Figure 17 shows that with the rotor turning, the downstream Cobra-probe measured the same harmonics as the HULMS. When the rotor was stopped the harmonics were not present,

demonstrating that the harmonics shown in the spectra are an artefact of the interaction between the turning rotor and the moving ship.

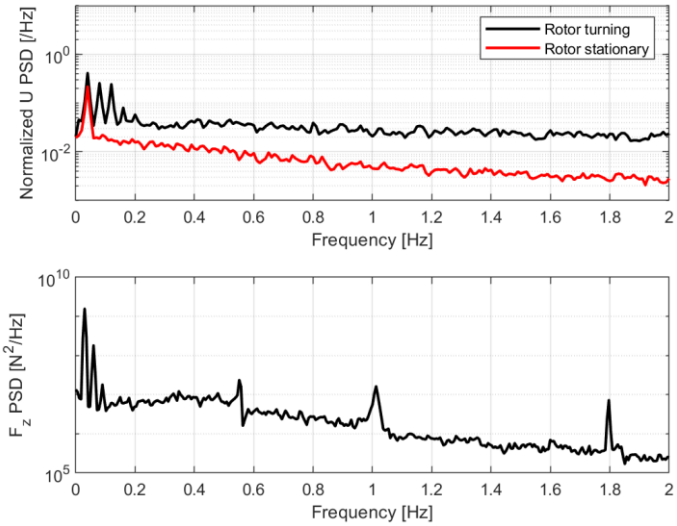

Figure 17: Cobra-probe (downstream) spectra with and without rotor turning at the nominal HH location in headwinds for a sinusoidally pitching ship. Cobra-probe data: top; HULMS data: bottom. Values are presented at equivalent FS.

7 Concluding Remarks

This paper has presented analyses of the impact of ship airwake upon helicopter aerodynamic loading. Both the NRC and UoL have applied their respective analysis approaches to measure the unsteady wind loading of the NATO-GR whilst immersed in the airwake of the NATO-GD for several ship motion types: static, sinusoidal pitching, regular 2-DOF, and realistic irregular 3-DOF ship motions. The HULMS, an experimental apparatus employed by the NRC, was used to study the features of unsteady rotor thrust. The VAD method, applied by UoL, considered CFD airwakes produced for simulation by NRC and measured the resultant unsteady loads of a flight dynamics model representative of the NATO-GR. The following conclusions have been drawn as a result of these analyses:

- When comparing across ship motion type, there was little difference observed in the mean loads but some variation in the RMS loads.

- It was found that the sinusoidal pitching motion resulted in the greatest differences from the static ship in mean and RMS loading, and the more complex realistic ship motion type showed less deviation. The greater variations for the sinusoidal pitch motion may be attributed to the larger deck displacements compared to other motion types.

- The spectra of the HULMS loads reflect the features present in the spectra of the airwake, including peaks caused by ship motion. However, these peaks occur below the traditional lower threshold for contributing to pilot workload of 0.2 Hz. Further work to confirm the validity of this lower limit would be beneficial.

- While simple motions with large amplitudes (the pitch case) showed extra energy added to the spectra at the ship motion frequency, more complex motion profiles with more realistic amplitudes did not add a significant measurable loading to the helicopter.

- The nature of the spectral peaks in the airwake due to ship motion is changed by the presence of the turning rotor. With the rotor turning, spectral superharmonics are present; with the rotor stopped, they are not.

Author Contact

Nicholas Fernandez Nicholas.Fernandez@liverpool.ac.uk,

Alanna Wall Alanna.Wall@nrc-cnrc.gc.ca,

Ieuan Owen I.Owen@liverpool.ac.uk,

Richard Lee Richard.Lee@nrc-cnrc.gc.ca,

Weixing Yuan Weixing.Yuan@nrc-cnrc.gc.ca,

Mark D. White mdw@liverpool.ac.uk.

Acknowledgements

The authors acknowledge the contributions of Mohamed Abdelhady for data conversion and the rest of the AVT-315 team.

References

1. Lumsden, R. B., Padfield, G. D., and Braby-Deighton, C. D., "Human Factors Challenges at the Helicopter-Ship Dynamic Interface," 1999 World Aviation Conference, San Francisco, CA, October 19-21, 1999. DOI: 10.4271/1999-01-5607.

2. Owen, I., White, M. D., Padfield, G. D., and Hodge, S. J., "A Virtual Engineering Approach to the Ship-Helicopter Dynamic Interface – a Decade of Modelling and Simulation Research at the University of Liverpool," *The Aeronautical Journa*l, Vol. 121, (1246), 2017, pp. 1833–1857. DOI: 10.1017/aer.2017.102.

3. Owen, I., Lee, R., Wall, A., and Fernandez, N., "The NATO Generic Destroyer – a Shared Geometry for Collaborative Research into Modelling and Simulation of Shipboard Helicopter Launch and Recovery," *Ocean Engineering*, Vol. 228, 2021, p. 108428. DOI: 10.1016/j.oceaneng.2020.108428.

4. Kääriä, C. H., Forrest, J. S., and Owen, I., "The Virtual AirDyn: A Simulation Technique for Evaluating the Aerodynamic Impact of Ship Superstructures on Helicopter Operations," *The Aeronautical Journal*, Vol. 117, (1198), 2013, pp. 1233–1248. DOI: 10.1017/S0001924000008836.

5. Comeau, P., Wall, A., Thornhill, E., McTavish, S., and Lee, R., "Supporting Shipboard Helicopter Flight Testing with Simulation and Metrics for Predicting Pilot Workload," *Journal of Defense Modeling and Simulation*, 2022. DOI: 10.1177/15485129221118937.

6. McTavish, S. A. M., Wall, A. S., and Lee, R. G., "A Methodology to Correlate Simulated Airwake Data and Unsteady Helicopter Load Measurements to Shipboard Helicopter Flight Test Data," 14th International Conference on Wind Engineering, Porto Alegre, Brazil, June 21-26, 2015.

7. NATO, "Standardized Wave and Wind Environments and Shipboard Reporting of Sea Conditions," STANAG 4194, 1983.

8. Yuan, W., Wall, A., and Lee, R., "Combined Numerical and Experimental Simulations of Unsteady Ship Airwakes," *Computers and Fluids*, Vol. 172, 2018, pp. 29-53. DOI: 10.1016/j.compfluid.2018.06.006.

9. Yuan, W., Wall, A., Thornhill, E., Sideroff, C., Mamou, M., and Lee, R., "CFD Aided Ship Design and Helicopter Operation," *Journal of Marine Science and Engineering*, Vol. 10, 2022. DOI: 10.3390/jmse10091304.

10. Du Val, R. W., and He, C., "Validation of the FLIGHTLAB virtual engineering toolset," *The Aeronautical Journal*, Vol. 122, (1250), 2018, pp. 519-555. DOI: 10.1017/aer.2018.12.

11. Wall, A., Lee, R., Barber, H., McTaggart, K., The NATO Generic Destroyer - a shared geometry for collaborative research into modelling and simulation of shipboard launch and recovery: source data posting on Open Science Canada, Feb 2021. Use title keywords at https://open.canada.ca/data/en/dataset

12. Leishman, J. G., *Principles of Helicopter Aerodynamics*. Cambridge University Press, Cambridge, 2006.

13. McRuer, D. T., "Interdisciplinary Interactions and Dynamic Systems Integration," *International Journal of Control*, Vol. 59, (1), 1994, pp. 3–12. DOI: 10.1080/00207179408923067.

14. Harrison, S., Wall, A., and Thornhill, E., "Assessing Pilot Response to Low-Frequency Disturbances: A Literature Review," CASI AERO 2019, Montreal, Quebec, May 14-16, 2019.

15. Fernandez, N., Watson, N., Owen, I., and White, M. D., "A Comparative Assessment of the NATO-GD and SFS2 Ship Airwakes and Their Influence upon Helicopter Aerodynamic Loading," Vertical Flight Society's 78th Annual Forum & Technology Display, Fort Worth, TX, May 10-12, 2022. DOI: 10.4050/F-0078-2022-17584.